Advances in Detector Instrumentation for PET

Andrea Gonzalez-Montoro[1], Muhammad Nasir Ullah[1], and Craig S. Levin[1–4]

[1]*Department of Radiology, Molecular Imaging Program at Stanford University, Stanford, California;* [2]*Department of Physics, Stanford University, Stanford, California;* [3]*Department of Electrical Engineering, Stanford University, Stanford, California; and* [4]*Department of Bioengineering, Stanford University, Stanford, California*

Learning Objectives: On successful completion of this activity, participants should be able to describe (1) the basics of PET detectors, including both indirect and direct 511 keV photon detection methods; (2) key detector performance parameters; and (3) the most relevant detector instrumentation advances during the last decade.

Financial Disclosure: Financial support was received from National Institutes of Health grant R01CA214669, Department of Energy grant DE-SC0021975, and an Emerson Collective award. Dr. Gonzalez-Montoro was partially supported by VALi+d Program for researchers in Postdoctoral Phase of the Ministry of Labor and Social Economy (Generalitat Valenciana) and the EU Social Fund. The authors of this article have indicated no other relevant relationships that could be perceived as a real or apparent conflict of interest.

CME Credit: SNMMI is accredited by the Accreditation Council for Continuing Medical Education (ACCME) to sponsor continuing education for physicians. SNMMI designates each *JNM* continuing education article for a maximum of 2.0 AMA PRA Category 1 Credits. Physicians should claim only credit commensurate with the extent of their participation in the activity. For CE credit, SAM, and other credit types, participants can access this activity through the SNMMI website (http://www.snmmilearningcenter.org) through August 2025.

During the last 3 decades, PET has become a standard-of-care imaging technique used in the management of cancer and in the characterization of neurologic disorders and cardiovascular disease. It has also emerged as a prominent molecular imaging method to study the basic biologic pathways of disease in rodent models. This review describes the basics of PET detectors, including a detailed description of indirect and direct 511-keV photon detection methods. We will also cover key detector performance parameters and describe detector instrumentation advances during the last decade.

Key Words: PET; scintillation detectors; semiconductor detectors; spatial and energy resolution; coincidence time resolution; CTR

J Nucl Med 2022; 63:1138–1144
DOI: 10.2967/jnumed.121.262509

PET imaging uses radioactive contrast agents for diagnosis and therapy monitoring of various medical conditions. PET imaging provides unique information on the cellular and molecular pathways of disease within the human body, complementary to that provided by γ-cameras and SPECT. PET is also quite often used for small-animal molecular imaging studies (*1*).

A PET study begins with the administration of a radioactive tracer. PET data acquisition is based on the coincident detection of millions of pairs of oppositely directed 511-keV photons, each of which results from the annihilation of a positron (a decay product of the tracer's radionuclide label) with its antiparticle (the electron present in all atoms of the molecules comprising patient tissues).

The resulting annihilation photons are detected using high-atomic-number, high-density, and thick radiation detectors typically arranged in a cylindric geometry (e.g., Fig. 1).

Received Feb. 14, 2022; revision accepted Apr. 22, 2022.
For correspondence or reprints, contact Craig S. Levin (cslevin@stanford.edu).

BASICS OF PET DETECTORS

The detection method for characterizing the incoming annihilation photons can be generally divided into 2 different categories: indirect and direct. In indirect (scintillation) detection, each incoming annihilation photon interacts within the scintillation crystal through photoelectric or Compton scatter interactions. The deposited energy is first converted into a cascade of visible (lower-energy) light photons and then into an electrical current using one or more photodetectors. This is the detection method used in all current commercially available PET systems (*2*). In direct detection, each incoming photon interaction is directly converted into electrical signals using semiconductor crystals. To date, this approach has been explored only in research (*3,4*). Each of these methods has its own advantages and limitations.

Indirect Detection Method (Scintillation Detection)

Scintillation detectors for PET use an inorganic crystal, which each incoming 511-keV annihilation photon interacts with (via Compton scatter or the photoelectric effect), producing a quickly ejected recoil electron. Each ejected electron travels through the material and ionizes it through coulombic interactions, creating a track of secondary electrons (*5*) that are liberated from the crystal's intrinsic electronic valence band into the conduction band. Through a subsequent deexcitation process in which those excited electrons drop into available energy states of the host crystal, or those of an impurity introduced into the crystal, the resulting ionization charge is converted to a flash of isotropically emitted visible light (*6*). The crystal is coupled to a photodetector element that collects the light and converts it into an electrical signal, followed by readout electronics (*7*).

Inorganic Scintillation Crystals Used in PET. Ideal inorganic scintillation materials should have a high effective atomic number (Z_{eff}) and density, and the resulting signals should have a fast rise and decay time, which are crucial for good coincidence timing resolution. To promote the generation of visible-light photons (i.e., optical photons), except for a few intrinsic scintillators such as bismuth germanium oxide (BGO), a small concentration of an impurity, called an activator, is introduced into the inorganic scintillation crystal (*8*).

A scintillator suitable for PET should have the following properties: high light yield, which is the number of optical photons

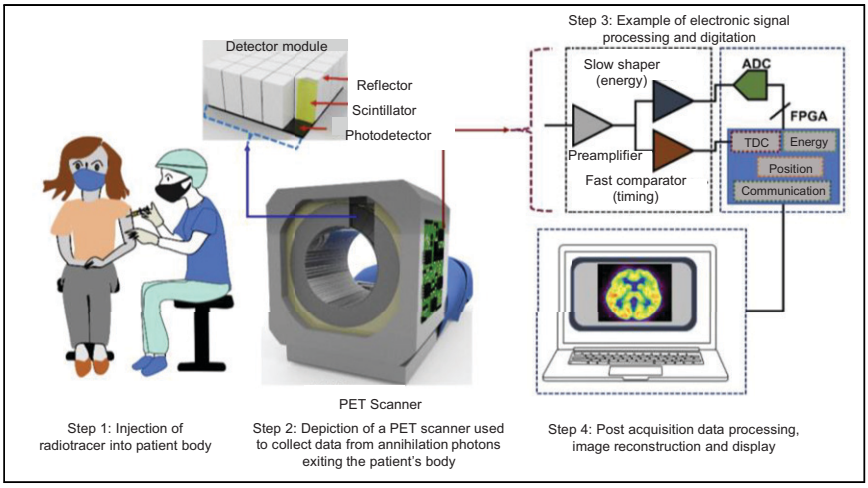

FIGURE 1. Illustration of PET imaging process: from left to right, radiolabeled tracer is injected into patient body, then PET scan is performed, and finally acquired annihilation photon data are processed to reconstruct images. ADC = analog-to-digital converter; FPGA = field programmable gate array; TDC = time-to-digital converter.

generated per unit of deposited energy from the interaction; good linearity, to ensure that the number of generated optical photons is proportional to the energy deposited by the incident radiation; transparency to the wavelength of its own emission spectra, to facilitate the transport of generated scintillation light to the photodetector; a high Z_{eff}, a high density and a relatively wide thickness (e.g., 2 cm), for favorable 511-keV interaction probability; a fast rise time and short decay time for the induced luminescence, to facilitate excellent temporal resolution and count rate performance; and a high refraction index, to promote total internal reflection off the crystal element sides and to increase the efficiency of light collection into the photodetector. Different inorganic scintillator materials have been used in PET detectors; Supplemental Table 1 (supplemental materials are available at http://jnm.snmjournals.org) summarizes the most commonly used inorganic scintillators and their properties for the purpose of indirect radiation detection. To promote good spatial resolution, energy resolution, and coincidence time resolution (CTR) performance, important aspects to consider in addition to high light yield, Z_{eff}, and density, and short rise and decay times, are the reflector applied to the scintillator crystal surfaces (to constrain the generated light photons within the crystal), the crystal surface condition (e.g., polished or rough), and the scintillator–photodetector coupling medium (*9*).

Although most modern PET systems are built using lutetium-based scintillation crystals (e.g., lutetium–yttrium oxyorthosilicate [LYSO]) because of their high light yield and excellent timing properties, there has been a recent resurgence of studies that explore BGO, especially its achievable timing properties using prompt luminescence emissions (*10*). As the field is moving toward scanners with a long axial field of view, BGO is especially attractive because of its significantly decreased production cost and increased Z_{eff} compared with lutetium-based crystals.

Regarding crystal configuration, there are 2 main geometries used in PET detectors, namely discrete array and monolithic, as depicted in Supplemental Figures 1A and 1B, respectively. Discrete crystal arrays are most commonly used in commercial PET scanners and comprise a matrix (i.e., array) of individual small rod-shaped scintillation elements, whereas the monolithic scintillator design (currently in only one commercial scanner design) consists of a large single piece of scintillation material, and therefore, there are no interelement gaps. Advantages and disadvantages of each configuration can be found in a previous publication (*11*).

Photodetectors Used in PET Scintillation Detectors. For the detection and conversion of the generated scintillation photons into measurable electrical signals, the scintillator is coupled to one or more photodetector elements. Generally, the photodetectors used in PET can be divided into 2 groups: photomultiplier tubes (PMTs) and silicon photomultipliers (SiPMs). PMTs are economically advantageous, have high gain and low noise, and are sensitive for light in the visible region of the electromagnetic spectra. However, they are relatively large, bulky, and affected by magnetic fields, making it impossible to use them in PET/MRI hybrid systems. Figure 2A shows the operation principle of PMTs (*6*). SiPMs are semiconductor (solid-state) light detectors with a very high gain, a low-temperature drift, a low operating voltage, an excellent temporal response, and an insensitivity to magnetic fields (*6*). They are much more compact than PMTs, with a pixel size on the order of the size of typical discrete crystal elements used in PET and with minimal dead area. Figure 2B depicts an SiPM array, zoomed in on the pixel internal circuit structure. The SiPM pixel comprises a 2-dimensional array of thousands of single-photon avalanche photodiodes operating in Geiger mode, known as microcells. When a single scintillation photon strikes a single microcell, a charge carrier (electron or hole, depending on the configuration) is generated with a certain probability and then accelerated through a strong electric field, triggering an avalanche in the gain region. The charge carriers from all microcells in each SiPM pixel are collected and summed in parallel, producing an output signal proportional to the number of impinging scintillation photons hitting that SiPM pixel that can be measured in real time. Depending on whether readout electronics are external to the devices or integrated within the sensor technology, SiPMs can be classified as either analog or digital, respectively (*12*).

Most newer-generation PET systems use SiPMs instead of PMTs (*13*). To provide accurate information on the incoming photon interaction location, energy, and arrival time, the factors

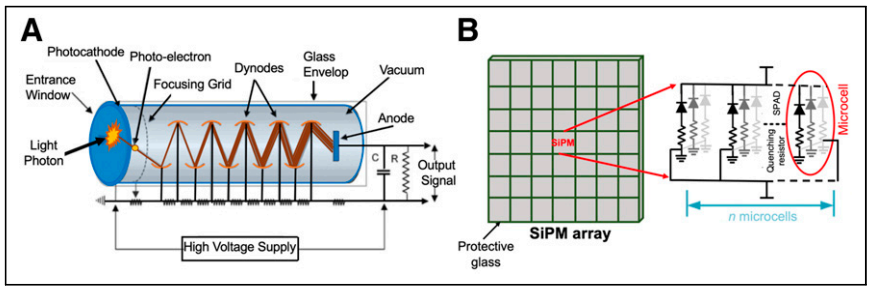

FIGURE 2. Schematic of PMT (A) and SiPM array (B), zooming on circuitry of one SiPM comprising 2-dimensional array of thousands of microcells. SPAD = single photon avalanche diode.

contributing to the SiPM noise and timing jitter, such as dark count rates, optical crosstalk, afterpulsing, and dead time, must be considered when designing SiPM-based systems (*14*).

For the crystal–photodetector coupling, it is better to use coupling media with refractive indices between those of the photodetector and the scintillator crystal to reduce light transmission losses. Regarding crystal–photodetector arrangement, for the discrete crystal design, photodetectors are commonly coupled to the small end of the crystal (end readout, Figs. 3A–3C). Nevertheless, designs attaching the photodetector to the entrance surface (Fig. 3D) (*9*), at the side surfaces (Fig. 3E) (*9*), or to both top and bottom surfaces (for 511-keV photon depth of interaction [DOI] positioning) (Fig. 3F) (*14*), or even covering the 4 lateral edges of a monolithic crystal (Fig. 3G) (the more common arrangement was depicted in Supplemental Fig. 1B, with the photodetector coupled to a large face of the crystal (*11*)), have also been studied, reporting good overall performance but, for some of the designs, at the cost of increasing the number of photodetectors or gaps between adjacent crystal elements (*14*).

There are 2 basic configurations to couple discrete scintillation crystals to photodetectors, namely light sharing and one-to-one coupling. In the light-sharing configuration, optical photons generated in one crystal element are collected in more than one photodetector, or a single photodetector collects the optical photons from more than one crystal element. The monolithic design (e.g., Supplemental Figs. 1B and 3F) involves substantial light sharing: for an interaction occurring in the center of the crystal, almost all SiPMs in the matrix receive signal. In the one-to-one crystal–photodetector coupling approach, each crystal element is optically isolated from its neighbors and coupled to its own photodetector pixel. In this configuration, the spatial resolution of such a detector is limited mainly by the width of the discrete crystal elements (*5*). The photodetector output signals may be read independently or multiplexed for fewer readout channels (*15*), as described in the following section. In the case of the monolithic crystal, the spread of scintillation light within the crystal leads to significant detector dead time at high count rates and spatial resolution degradation near the edges (*16*), which have a negative effect on timing performance throughout the crystal since there is an increased variance in the photon arrival time determination (*17*).

Front-End Readout Electronics for PET Scintillation Detectors. The front-end readout and data acquisition electronics are responsible for processing and digitizing the photodetector output signals and transmitting those digitized signals to a workstation (personal computer) for further processing and image reconstruction. Analog SiPMs provide analog electrical signals. High-speed analog-to-digital converters are used to accurately digitize these analog signals (e.g., Fig. 1C), from which one can extract the crystal location, energy, and arrival time of the photon interaction. Because of their flexibility, reliability, and cost effectiveness, field-programmable gate arrays (e.g., Fig. 1C) are the digital signal hardware units most often applied to control, receive, and process the digitized data from the analog-to-digital converters before transmitting to the personal computer for further software analysis and image reconstruction.

In terms of signal-to-noise ratio (SNR), the best approach to extracting 511-keV photon interaction position and temporal resolution is to read every single element in the photodetector matrix individually. However, this typically implies digitizing a huge number of signals, which is challenging, costly, and requires complex readout and data acquisition schemes. To address this challenge, multiplexing schemes that merge two or more photodetector output signals have been implemented (*18*). Multiplexing reduces the overall readout channel count but at the cost of signal integrity and postprocessing computational burden. For a readout design that combines several output channels, the exact interaction position of the 511-keV photon within the detector element that generated the electronic signal is unknown at the output of a multiplexed readout chain and therefore requires the application of algorithms or techniques (*19*) at the postprocessing stage to extract information such as photon interaction position, energy, and timing.

The most popular multiplexing methodology is Anger logic (the widely used in NaI-based γ-cameras), in which all photodetector signals are combined, such as through a resistive network (*20*). However, such multiplexing of output signals may require significant light sharing between the photodetectors, requiring a high light-output scintillator to obtain good spatial resolution. Thus, there is a tradeoff between the degree of multiplexing and the overall detector performance (*20*). Nevertheless, this multiplexing scheme provides the advantage of reducing the number of output channels and the overall complexity of a system but typically affects key performance parameters such as spatial, timing, and energy resolutions and count-rate performance. An alternative approach is to use capacitive multiplexing schemes or a hybrid multiplexing scheme in which resistive and capacitive networks are used in parallel (*21*). These different types of multiplexing schemes have a goal of improving one or more key parameters and can be adopted accordingly depending on the application.

Although some examples have been given, photodetector signal multiplexing in PET system design is generally an open area in which continued research is required to come up with optimized solutions for given detector configurations. For the readout schemes described, system designers often use application-specific integrated circuit (ASIC) chips—the so-called system on a chip (*22*)—which are customized for a particular use. ASIC readouts possess a small footprint and can be used to read, preprocess, and digitize each SiPM photodetector element independently or the resulting channels after multiplexing. Because of the customized design of ASICs for a specific type of detector and requirement, they often can yield performance parameters superior to those from readout circuits built using discrete components (*23*).

More recently, approaches based on artificial intelligence have been proposed for

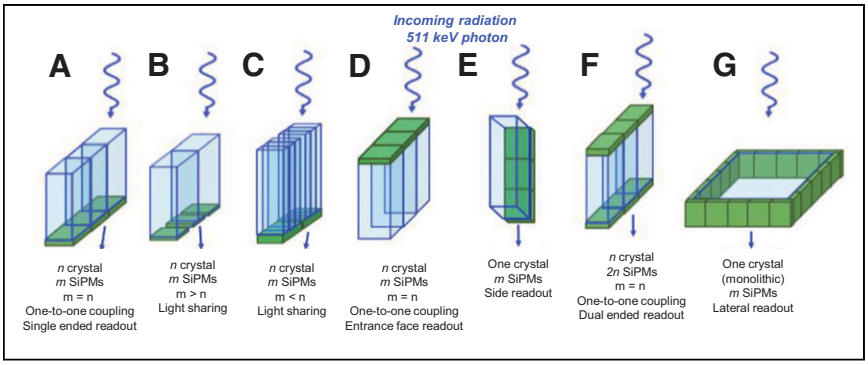

FIGURE 3. Schematic of different scintillation crystal–photodetector coupling approaches. End readout configurations with one-to-one coupling (A), light sharing (B and C), one-to-one coupling but with SiPMs on entrance face (D), side readout (E), dual-ended readout (F), and lateral readout (G) (a more common configuration is depicted in Supplemental Fig. 1B).

3-dimensional photon interaction positioning and time stamp estimation in PET for highly multiplexed readout schemes (*24*). Preliminary experiments have shown promising results (*25*).

Direct Detection Method

Semiconductor detectors are commonly used in the field of radiation detection for direct conversion of the incoming radiation into electrical signals (without the intermediate process of creation, transport, and collection of light) and are currently under research for use in PET (*3,4,26*). In semiconductor photon detectors, the 511-keV photon interaction physics are exactly the same as in the indirect detection (scintillation) case, in which the ionizing interactions create a track of electron–hole pairs. However, what differs is the signal formation and collection process. In a semiconductor detector, under the influence of an applied bias voltage on electrodes deposited on opposing sides of the crystal, the mobile charge carriers drift toward and induce a current on either electrode (electrons drift toward the anode whereas holes drift toward the cathode) as depicted in Supplemental Figure 2 (*4*). The integral of induced current over time provides the total induced charge on each electrode, which, aside from charge-attenuating effects, is directly proportional to the energy of the 511-keV photon interaction. The resulting current signal is read through highly sensitive and low-noise electronic circuitry. Typically, the first component of the front-end readout circuitry chain is a charge-sensitive amplifier. The basic function of the charge-sensitive amplifier is to integrate the current signal and convert it into a voltage signal, as well as to match electrical impedance between the detector and subsequent electronics (*4*). The charge-sensitive amplifier is typically followed by a shaping amplifier, which amplifies the signal and filters out the noise contents from the output signal of the charge-sensitive amplifier to improve SNR. The shaping amplifier also plays the important role of quickly decaying the signal down to baseline to avoid pile-up issues and make the data acquisition system ready for processing of subsequent signals without compromising the precision of extraction of time and energy information from the signal. The output of the shaping amplifier can be fed to an analog-to-digital converter for signal digitization and postprocessing.

Because of a single-step 511-keV photon-induced ionization-to-current conversion, semiconductor detectors exhibit a greatly decreased (compared with scintillation-based radiation detectors) statistical variation in signal amplitude as a function of the photon energy, thus yielding more precise energy measurements (i.e., higher energy resolution), which are highly desirable in imaging applications. However, one of the major limitations of semiconductor photon detectors is poor CTR, which limits the use of semiconductor detectors in the design of time-of-flight (TOF) PET scanners (*27*). The poorer temporal precision of semiconductor radiation detectors than of scintillation detectors results from the fact that the output signal is produced by the drift of charge, which is much slower and has larger temporal variation than the propagation and collection of light. Despite these drawbacks, there is still the possibility of using semiconductor radiation detectors for the design of high-resolution PET scanners (*3,28*) or in other applications in which timing performance is not of the utmost importance. So far, there are no clinical PET systems using semiconductor-based detectors.

To be used as an effective radiation detector for PET, a semiconductor material must have high Z_{eff} and density and be at least a few centimeters thick for highly efficient detection of 511-keV photons; it also should have high resistivity and low leakage current and should yield a high number of electron–hole pairs per interaction for the best detector SNR. The semiconductor radiation crystals that have been most often studied for PET detectors are cadmium zinc telluride (*4,29*) and cadmium telluride. Additionally, thallium bromide has also been recently studied (*30*). The basic properties of these 3 semiconductor detectors are summarized in Supplemental Table 2.

PET DETECTOR PERFORMANCE PARAMETERS

Intrinsic Spatial Resolution

The intrinsic spatial resolution of a PET detector is defined by the spatial spread of detected annihilation photon counts measured by stepping a positron point source across the surface of PET detectors that are operated in electronic coincidence (to collect the resulting oppositely directed annihilation photons), also known as the coincidence point-spread function (CPSF). The resolution is defined as the full width at half maximum (FWHM) of a gaussian fit to the CPSF and is usually characterized in 3 dimensions: 2 planar coordinates (x,y) in combination with the DOI coordinate (z) within the crystal.

At the system level, the intrinsic spatial resolution of the PET detector is an important parameter affecting PET image quality and, in the discrete crystal design, is affected mainly by the crystal element dimensions and the positioning algorithm used to retrieve the coordinates. Positron range and annihilation photon acollinearity variations also contribute to the measured (x,y) CPSF (*5*). In detector designs without signal multiplexing, the contribution from the detector is roughly half the width of the crystal element; in light-sharing and signal-multiplexing designs, an additional decoding term should be applied (*7*). For the overall (x,y) PET system spatial resolution, one would multiply intrinsic spatial resolution by an additional blurring factor because of the imperfect image reconstruction process, as shown in Equation 1. The reconstructed image voxel size is usually chosen to be roughly one third to one half the intrinsic resolution (*31*). Annihilation photon acollinearity depends on scanner diameter. Positron range depends on the positron-emitting radionuclide and the tissue traversed by the positron. The contribution from the detector depends on the detector element width.

$$R_{int} = \sqrt{\left(\frac{R_{det}}{2}\right)^2 + R_{pos}^2 + b^2 + 0.0044 \cdot R_{acol}^2}, \qquad \text{Eq. 1}$$

where R_{int} is intrinsic spatial resolution, R_{det} is the contribution from the detector, R_{pos} is the positron range, b is the blurring factor, and R_{acol} is annihilation photon acollinearity. Submillimeter (x,y) intrinsic resolution has been achieved for both indirect and direct detection methods. Supplemental Figure 3 shows examples of PET systems with intrinsic resolution of less than 1 mm (*3,32*). Supplemental Figure 3A depicts an example of indirect detection of the measured PSF across 2 opposing detector modules, each consisting of 8×8 arrays of $0.9 \times 0.9 \times 1\,mm^3$ LYSO scintillation crystals coupled to a position-sensitive avalanche photodiode. An average CPSF of 0.84 ± 0.02 mm was measured; the figure was extracted from a previous publication (*33*). Supplemental Figure 3C shows an example of the direct detection method using a monolithic CZT crystal arranged edge-on with respect to incoming photons, with intrinsic resolution determined by the 1-mm pitch of the anode electrode, which was segmented into strips; the reported CPSF averaged over 3 anode strips was 0.78 ± 0.1 mm FWHM, including the 250-μm diameter of the point source. This figure was extracted from a previous publication (*34*).

Regarding the monolithic crystal-based detector design, an additional challenge is the truncation of scintillation light at the edges, which degrades the spatial, timing, and energy resolutions in these regions (*7*). Several approaches to mitigating this effect have been tested, such as different crystal surface treatments (e.g., covering the edges with an optical absorber) or novel photodetector arrangements (*9,11*). Moreover, monolithic detectors require 2-dimensional calibration procedures to estimate the 511-keV photon interaction position within the scintillator. These calibration procedures are usually based on hardware collimation methods in which a physically collimated beam source is moved across the front face of the scintillator to generate look-up tables that are used to decode the measured positions into metric units (*5*). Supplemental Figure 3B shows an example of a calibration pattern acquired using a 15-mm-thick LYSO monolithic crystal and a collimated array of ^{22}Na sources with 1.5-mm pitch. The collimator had 30-mm thickness and drilled holes 1.2 mm in diameter. The bottom panel of Supplemental Figure 3B shows the count histogram along the columns in the image of the data inside the red band, achieving an average (*x,y*) spatial resolution of 0.82 ± 0.02 mm after taking into account the hole diameter, with significant degradations observed within a few millimeters from all 4 edges (*33*).

A high-sensitivity PET system design is desirable for realizing both high spatial resolution and reconstructed image SNR. This can be achieved by using scintillation crystals at least 2 cm long (thick) for high-efficiency detection of 511-keV photons. However, nearly all commercially available PET detectors do not measure the DOI of the photon interaction. This lack of DOI information can produce significant limitations in positioning annihilation photon interactions due to a parallax error that occurs when incoming annihilation photons enter the detectors at oblique angles and interact at varying depths within the crystals. This leads to increased spatial-resolution blurring as the source moves outward from the center, radially.

However, retrieving DOI information is not straightforward and usually requires additional scintillator layers (e.g., phoswich approaches (*35,36*)) or photodetector elements (dual-end readout methods)—or special crystal surface treatments and reflectors (*9,36*)—and additional readout channels, thus increasing manufacturing cost and system complexity (*8*). The drawbacks of most of these DOI methods is that they can determine only one DOI, representing a problem when the photon interacts more than once in the detector crystals (intercrystal scatter) before depositing all its energy (i.e., a Compton scatter followed by a photoelectric absorption), which is roughly 2- to 3-fold more likely to occur than a single photoelectric interaction for small (<4 mm in width) crystals. To address this problem, some advanced detector designs enable determination of *x, y,* and *z* coordinates when there is more than one 511-keV photon interaction (*3,32*), enabling an accurate estimate of the first interaction for improved reconstructed image quality and accuracy (*37*).

Energy Resolution

The energy resolution is a measure of the detector's ability to distinguish between photon interactions at different energies and represents the precision with which a PET detector can measure the deposited energy of the photon interaction. It is quantified by the FWHM of a gaussian fit to the photopeak observed in the measured spectrum of detected photon energies. Good energy resolution helps to filter out 511-keV photons that have undergone Compton scatter in the patient tissues before being detected, since it allows the application of a narrow energy window for rejection of these scattered coincidences, thus improving image contrast and accuracy while still being able to collect high count statistics in the measured photopeak. Semiconductor detectors provide better energy resolution because of low statistical variation in signal amplitude as a function of photon energy. For the sake of comparison of direct and indirect detection, the energy spectrum of a ^{22}Na radiation source acquired using a 3 × 3 × 10 mm^3 lutetium–gadolinium orthosilicate scintillator crystal element coupled to an SiPM (*9*), and a 39 × 39 × 5 mm^3 cadmium zinc telluride semiconductor detector crystal arranged edge-on with respect to incoming photons (*38*), are shown in Supplemental Figures 4A and 4B, respectively. In discrete and monolithic crystal array–based detectors, the energy resolution depends on the scintillator light yield, light collection efficiency variations as a function of annihilation photon DOI, the dimensions of the crystal element and its optical coupling to the photodetector, properties of the latter such as photon detection efficiency, and the noise level of the electronic readout.

CTR

The CTR of a PET system defines the uncertainty in measuring the arrival time difference between photons for each annihilation photon pair of a coincidence event, over many events. The CTR is determined by several factors, including the intrinsic properties of the scintillation crystal (light yield, rise and decay times), reflective materials applied to the crystal, the geometry of the crystal, the number of scintillation photons collected by the photodetector, crystal-to-photodetector coupling configurations, photodetector detection efficiency and noise properties, and the readout electronics chain (*39*). Achieving precise CTR allows one to constrain the location of each annihilation event along the system lines of response using the technique known as TOF (*2*). Using TOF information, each event is placed closer to its true origin along the line of response connecting 2 coincidence detector elements in a PET system during the image reconstruction process, thus improving the reconstructed image SNR (Eq. 2) (*9*).

$$SNR = \left(\frac{D}{\Delta X}\right)^{1/2} = \left(\frac{2 \cdot D}{c \cdot \Delta T}\right)^{1/2}, \qquad \text{Eq. 2}$$

where $\Delta X = (c \cdot \Delta T/2)$ is the annihilation coordinate uncertainty along each line of response, c is the speed of the light, ΔT is *CTR,* and D is the imaging subject diameter, assuming it is circular. As an example, if the CTR improves from 400 to 100 ps, then from Equation 1, a gain in reconstructed image SNR of a factor of $\sqrt{4}$ (=2) is expected.

The image SNR boost using TOF can be exploited to improve lesion visualization and the accuracy of uptake measurements or reduce the required dose or the scan time. The design of TOF PET scanners requires careful consideration of the scanner photon sensitivity and the CTR performance (*39,40*). Supplemental Figure 4C shows an example of the measured time difference (i.e., coincidence time) spectrum, which is again typically quantified by the FWHM, using a detector design based on a 3 × 3 × 10 mm^3 lutetium–gadolinium orthosilicate scintillator crystal element side-coupled to a 3 × 3 mm^3 SiPM (*9*).

Count-Rate Performance

Count rate is defined as the number of events recorded by a detector per unit of time. The count-rate capability of PET systems is constrained because a large number of incoming photon events has to be detected and processed by a finite number of detector channels, each channel requiring a certain processing time

depending on the detector and readout electronics design. Thus, the total number of counts that can be collected within a reasonable time frame is limited (*40*). In an ideal PET system, the net count rate would increase linearly with increasing activity in the field of view. However, real systems experience count losses due primarily to dead time caused by event pile-up effects. These effects must be estimated accurately and corrected in order for quantitative PET studies to be performed; in this regard, several methods have been proposed to alleviate count-rate losses (*41*). With the introduction of SiPM-based detectors, the pile-up and resulting dead time and loss in quantitative accuracy observed at high count rates is reduced when compared with previous PMT-based scanners (*42*).

Count-rate measurements do not directly indicate image SNR in the presence of random and Compton scatter coincidence backgrounds. Instead, the noise-equivalent count rate figure of merit is used, providing a standard measure of the SNR of a PET system (*40*).

DISCUSSION

Currently, PET imaging is a valuable molecular imaging technique and is used clinically to yield tailored diagnostic and prognostic information. Advances in PET detector design and instrumentation in the last decade have led to significant improvements in PET image quality and accuracy. Supplemental Table 3 summarizes the main performance parameters of commercial TOF PET scanners (*2*). However, there are potentially a few directions for improvement: commercially available clinical PET scanners are still not efficient in detecting 511-keV photon pair coincidences (i.e., photon sensitivity) relative to theoretic scanner designs (*43*) and offer limited spatial resolution (~4 mm at the system center, which degrades away from the center).

One direct (but costly) approach to improving PET system sensitivity is that of the Explorer collaboration (*44*)—as well as other designs (*45*)—to improve the system geometric efficiency by greatly increasing its axial length. The axial length of most commercially available PET systems ranges between 15 and 26 cm, exhibiting sensitivities of 0.6%–2% for the 70-cm-long National Electrical Manufacturers Association line source measurement. For reducing the cost of PET systems with a long axis, there has been recent significant interest in BGO (*10*).

Another indirect option to enhance PET system sensitivity is to improve CTR and, thus, the precision of photon TOF information during the reconstruction process, which provides an effective sensitivity boost by enhancing reconstructed image SNR. The best state-of-the-art scanner achieves an approximately 214-ps CTR (*46*). However, with progress in the development of SiPMs (*12,13*), high-end PMTs, and scintillators, a CTR at or below a 100-ps FWHM may be achievable in future-generation TOF PET systems (*4,9*).

PET system spatial resolution and sensitivity improvements have been proven useful to better characterize and quantify lesions or to reduce the radiation dose or scanning time. To improve the spatial resolution of PET scanners, one may use smaller crystal elements along with sensitivity improvements to realize the desired higher resolution with good image SNR. Recently, artificial-intelligence algorithms are being explored for use with PET instrumentation (*24*). For example, they have been used to achieve homogeneous submillimetric resolution in the entire field of view using a monolithic-crystal–based design (*11*).

CONCLUSION

PET constitutes the molecular imaging technique of excellence in nuclear medicine. However, to further extend the use of PET, some instrumentation improvements need to be accomplished. These advancements include reaching high 3D spatial resolution (in the range of ~1−2 mm); achieving CTR values below 100 ps to enable the inclusion of precise TOF information during the reconstruction process; and maximizing photon detection sensitivity. The present review covers these points by describing the basics of PET detector technology, the most relevant instrumentation milestones completed during the last decade, and the future of PET detector technology.

ACKNOWLEDGMENT

We gratefully acknowledge the feedback provided by our Molecular Imaging Instrumentation Laboratory (MIIL) members.

REFERENCES

1. Phelps ME. Positron emission tomography provides molecular imaging of biological processes. *Proc Natl Acad Sci USA.* 2000;97:9226–9233.
2. Surti S, Karp JS. Update on latest advances in time-of-flight PET. *Phys Med.* 2020; 80:251–258.
3. Abbaszadeh S, Levin CS. New-generation small animal positron emission tomography system for molecular imaging. *J Med Imaging (Bellingham).* 2017;4:011008.
4. Gu Y. *High-Resolution Small Animal Positron Emission Tomography System Based on 3-D Position-Sensitive Cadmium Zinc Telluride Photon Detectors.* Stanford University; 2014:26–40.
5. Levin CS, Hoffman EJ. Calculation of positron range and its effect on the fundamental limit of positron emission tomography system spatial resolution. *Phys Med Biol.* 1999;44:781–799.
6. Bizarri G. Scintillation mechanisms of inorganic materials: from crystal characteristics to scintillation properties. *J Cryst Growth.* 2010;312:1213–1215.
7. Bailey DL, Karp JS, Surti S. Physics and instrumentation in PET. In: Bailey DL, Townsend DW, Valk PE, Maisey MN, eds. *Positron Emission Tomography.* Springer; 2005:13–39.
8. Melcher CL. Scintillation crystals for PET. *J Nucl Med.* 2000;41:1051–1055.
9. Gonzalez-Montoro A, Pourashraf S, Lee MS, Cates JW, Levin CS. Study of optical reflectors for a 100ps coincidence time resolution TOF-PET detector design. *Biomed Phys Eng Express.* 2021;7:65008.
10. Gonzalez-Montoro A, Pourashraf S, Cates JW, Levin CS. Cherenkov radiation-based coincidence time resolution measurements in BGO scintillators. *Front Phys (Lausanne).* 2022;10:816384.
11. Gonzalez-Montoro A, Gonzalez AJ, Pourashraf S, et al. Evolution of PET detectors and event positioning algorithms using monolithic scintillation crystals. *IEEE Trans Radiat Plasma Med Sci.* 2021;5:282–305.
12. Schaart DR, Charbon E, Frach T, Schulz V. Advances in digital SiPMs and their application in biomedical imaging. *Nucl Instrum Methods Phys Res A.* 2016;809: 31–52.
13. Acerbi F, Gundacker S. Understanding and simulating SiPMs. *Nucl Instrum Methods Phys Res A.* 2019;926:16–35.
14. Berg E, Cherry SR. Innovations in instrumentation for positron emission tomography. *Semin Nucl Med.* 2018;48:311–331.
15. Cherry SR, Jones T, Karp JS, Qi J, Moses WW, Badawi RD. Total-body PET: maximizing sensitivity to create new opportunities for clinical research and patient care. *J Nucl Med.* 2018;59:3–12.
16. Downie E, Yang X, Peng H. Investigation of analog charge multiplexing schemes for SiPM based PET block detectors. *Phys Med Biol.* 2013;58:3943–3964.
17. Kim H, Kao C-M, Hua Y, Xie Q, Chen C-T. Multiplexing readout for time-of-flight (TOF) PET detectors using striplines. *IEEE Trans Radiat Plasma Med Sci.* 2021;5:662–670.
18. LaBella A, Petersen E, Cao X, Zeng X, Zhao W, Goldan A. 36-to-1 multiplexing with Prism-PET for high resolution TOF-DOI PET [abstract]. *J Nucl Med.* 2021; 62(suppl 1):38.
19. Chinn G, Olcott PD, Levin CS. Sparse signal recovery methods for multiplexing PET detector readout. *IEEE Trans Med Imaging.* 2013;32:932–942.
20. Hobson PR. Measurement Instrumentation and Sensors Handbook: Electromagnetic, Optical, Radiation, Chemical, and Biomedical Measurement, by J.G. Webster and H. Eren. *Contemp Phys.* 2015;56:505–506.
21. Park H, Ko GB, Lee JS. Hybrid charge division multiplexing method for SiPM-based high-resolution PET detectors. *Phys Med Biol.* 2017;62:4390–4405
22. Gao W, Gao D, Wei T, Hu Y. Survey of front-end readout ASICs for positron emission tomography imaging. *Guti Dianzixue Yanjiu Yu Jinzhan/Res Progress Solid State Electronics.* 2012;32:590–599.

23. Nadig V, Schug D, Weissler B, Schulz V. Evaluation of the PETsys TOF-PET2 ASIC in multi-channel coincidence experiments. *EJNMMI Phys.* 2021; 8:30.
24. Ullah MN, Levin CS. Application of artificial intelligence in PET instrumentation. *PET Clin.* 2022;17:175–182.
25. Sitek A, Ahn S, Asma E, et al. Artificial intelligence in PET: an industry perspective. *PET Clin.* 2021;16:483–492.
26. Takei T, Shiga T, Morimoto Y, et al. A novel PET scanner with semiconductor detectors may improve diagnostic accuracy in the metastatic survey of head and neck cancer patients. *Ann Nucl Med.* 2013;27:17–24.
27. Ullah MN, Pratiwi E, Cheon J, Choi H, Yeom JY. Instrumentation for time-of-flight positron emission tomography. *Nucl Med Mol Imaging.* 2016;50:112–122.
28. Abbaszadeh S, Gu Y, Reynolds PD, Levin CS. Characterization of a sub-assembly of 3D position sensitive cadmium zinc telluride detectors and electronics from a sub-millimeter resolution PET system. *Phys Med Biol.* 2016;61:6733–6753.
29. Abbaspour S, Mahmoudian B, Islamian JP. Cadmium telluride semiconductor detector for improved spatial and energy resolution radioisotopic imaging. *World J Nucl Med.* 2017;16:101–107.
30. Ariño-Estrada G, Mitchell GS, Kwon SI, et al. Towards time-of-flight PET with a semiconductor detector. *Phys Med Biol.* 2018;63:04LT01.
31. Groll AN. *Hybrid Pixel-Waveform Semiconductor Detectors: Novel Detector Readout for Semiconductor PET Imaging of Small Animal Neurodegenerative Models.* Dissertation. University of Illinois at Urbana-Champaign; 2017.
32. Shakirin G, Crespo P, Fiedler F, Wagner A, Enghardt W. Optimum voxel size for reconstruction of in-beam PET data. In: *2008 IEEE Nuclear Science Symposium Conference Record.* IEEE; 2008:5066–5069.
33. Hsu DFC, Freese DL, Reynolds PD, Innes DR, Levin CS. Design and performance of a 1 mm^3 resolution clinical PET system comprising 3-D position sensitive scintillation detectors. *IEEE Trans Med Imaging.* 2018;37:1058–1066.
34. Gu Y, Matteson JL, Skelton RT, et al. Study of a high-resolution, 3D positioning cadmium zinc telluride detector for PET. *Phys Med Biol.* 2011;56:1563–1584.
35. González-Montoro A, Sánchez F, Bruyndonckx P, Cañizares G, Benlloch JM, González AJ. Novel method to measure the intrinsic spatial resolution in PET detectors based on monolithic crystals. *Nucl Instrum Methods Phys Res A.* 2019; 920:58–67.
36. Ullah MN, Pratiwi E, Park JH, Lee K, Choi H, Yeom J-Y. Wavelength discrimination (WLD) TOF-PET detector with DOI information. *Phys Med Biol.* 2020;65: 055003.
37. Ullah MN, Park JH, Pratiwi E, Kim GB, Yeom J-Y. Wavelength discrimination (WLD) detector optimization for time-of-flight positron emission tomography with depth of interaction information. *Nucl Instrum Meth A.* 2020;982:164498.
38. Ullah MN, Pratiwi E, Park JH, et al. Studies on sub-millimeter LYSO:Ce, Ce:GAGG, and a new Ce:GFAG block detector for PET using digital silicon photomultiplier. *Nucl Instrum Methods Phys Res A.* 2018;911:115–122.
39. Pratx G, Levin CS. Bayesian reconstruction of photon interaction sequences for high-resolution PET detectors. *Phys Med Biol.* 2009;54:5073–5094.
40. Pourashraf S, Gonzalez-Montoro A, Won JY, et al. Scalable electronic readout design for a 100 ps coincidence time resolution TOF-PET system. *Phys Med Biol.* 2021;66:85005.
41. Cherry SR, Dahlbom M. PET: Physics, instrumentation, and scanners. *PET Springer*, 2004;1–124.
42. Wagatsuma K, Miwa K, Sakata M, et al. Comparison between new-generation SiPM-based and conventional PMT-based TOF-PET/CT. *Phys Med.* 2017;42: 203–210.
43. Vandenberghe S, Moskal P, Karp JS. State of the art in total body PET. *EJNMMI Phys.* 2020;7:35.
44. Usman S, Patil A. Radiation detector deadtime and pile up: a review of the status of science. *Nucl Eng Technol.* 2018;50:1006–1016.
45. Badawi RD, Shi H, Hu P, et al. First human imaging studies with the EXPLORER total-body PET scanner. *J Nucl Med.* 2019;60:299–303.
46. Ullah MN, Levin CS. Application of artificial intelligence in PET instrumentation. *PET Clin.* 2022;17:175–182.